Film forming hybrid acrylic/ZnO latexes with excellent UV absorption capacity

Miren Aguirre [a], Mariano Barrado [b], Maider Iturrondobeitia [c], Ana Okariz [d], Teresa Guraya [c], Maria Paulis [a], Jose Ramon Leiza [a]

[a] POLYMAT, Kimika Aplikatua saila, Kimika Zientzien Fakultatea, University of the Basque Country UPV/EHU, Joxe Mari Korta Zentroa, Tolosa Hiribidea 72, 20018 Donostia-San Sebastián, Spain

[b] SGIker, University of the Basque Country UPV/EHU, Joxe Mari Korta Zentroa, Tolosa Hiribidea 72, 20018 Donostia-San Sebastián, Spain

[c] eMERGE and Department of Mining and Metallurgical Engineering and Materials Science, University of the Basque Country UPV/EHU, P_ Rafael Moreno Pitxitxi, 3, 48013 Bilbao, Spain

[d] eMERGE and Department of Applied Physics I, University of the Basque Country UPV/EHU, P_ Rafael Moreno Pitxitxi, 3, 48013 Bilbao, Spain

Abstract

Acrylic/ZnO hybrid latexes were synthesized through a two-step emulsion polymerization process. First, a hybrid seed was synthesized by miniemulsion polymerization, which contained all the hydrophobically modified ZnO nanoparticles. Subsequently, this hybrid seed was employed in a seeded semibatch emulsion copolymerization yielding high solids content hybrid latexes (40 wt%). Cryo-transmission electron microscopy (cryo-TEM) demonstrated that the dispersion of the ZnO nanoparticles in the initial miniemulsion was not homogeneous, which led to a hybrid seed with two populations, polymer particles containing ZnO and pristine polymer particles. After the second step of polymerization barely the same morphology was obtained. Nevertheless, it was proved by electron tomography (3D-TEM) that the ZnO nanoparticles were encapsulated in the polymer particles. The hybrid films containing ZnO presented a superior UV absorption capacity than their counterpart hybrid acrylic/CeO$_2$ prepared following the same strategy.

1. Introduction

In the last two decades the incorporation of nanosized inorganic materials into organic polymer matrix has attracted the interest of scientists in academia and industry. This is mainly due to the synergetic effects observed when combining the properties of the inorganic materials (inertness, chemical resistance, temperature resistance, weather and UV resistance, hardness..) with the polymeric ones (processability, flexibility, toughness, gloss, curing…) [1].

Miniemulsion polymerization is a powerful technique to obtain hybrid organic–inorganic materials with encapsulated morphology. This morphology is attractive due to the advantages that it provides to the final hybrid material. For instance, better dispersion of the inorganic material in the polymeric matrix, improved stability against aggregation of the nanofillers, protection of the filler from the outside components (environment) or improvements in many properties such as mechanical, optical or barrier [2], [3], [4], [5], [6]. However, there are three main aspects to take into consideration when encapsulating inorganic nanoparticles by miniemulsion polymerization. The first one is the wettability of the nanoparticles in the monomer phase. This requires the modification of the naturally hydrophilic surface of the inorganic material. The second one is the emulsification process, which will define the size of the monomer droplets. And the last one, the aspect ratio and the size of the nanofiller [7], [8], [9], [10], [11]. The encapsulation of the inorganic material by miniemulsion polymerization is not always achieved; its success being governed by thermodynamic and kinetic considerations [12], [13].

Recently, we have shown that CeO_2 nanoparticles were successfully encapsulated into high solids content acrylic latex binders by means of a two-step semibatch polymerization strategy [14]. The first step consisted on the production of a hybrid seed by batch miniemulsion polymerization using hydrophobically modified CeO_2 nanoparticles, and the second step comprised a seeded semibatch process where the feed was either a preemulsion of monomer, for low CeO_2 loadings [14], [15], or a hybrid miniemulsion, for higher CeO_2 loadings [16].

This two-step semibatch polymerization strategy can be used to encapsulate other metal oxides or inorganic materials with potential applications in fields that include UV-blocking clear coats, solar cells and anticorrosive coatings among others. Another interesting metal oxide nanoparticle that can be incorporated into polymer matrices is zinc oxide (ZnO). ZnO nanoparticles present a wide band gap energy (3.4 eV) and large excitation binding energy (60 mV), which make them ideal for catalytic, optical and electrical applications [17], [18], [19], [20], [21].

ZnO nanoparticles have been incorporated into organic–inorganic nanocomposite waterborne dispersions using different polymerization strategies and polymeric matrices [19], [22], [23], [24], [25], [26] and for a wide range of applications. Dhoke et al. [25] directly added a dispersion of ZnO nanoparticles to an aqueous commercial alkyd resin dispersion and observed that small amounts (0.01–0.03 wt%) of ZnO nanoparticles improved corrosion and mechanical properties (scratch and abrasion resistances). Xiong et al. [26] blended styrene/butyl acrylate latexes and nanoZnO dispersions in substantially higher amounts (up to 9 wt%) and analyzed the effect of ZnO particle size on mechanical and optical (UV and NIR shielding) properties. They found that the better the dispersion

of ZnO in the matrix and the smaller the size of ZnO nanoparticles, the better the properties achieved by the hybrid composite materials.

Other authors used ZnO nanoparticles as Pickering stabilizers in oil-in-water dispersions. Thus, Chen et al. [23] showed that the morphology of ZnO/PS hybrid dispersions changed depending on the hydrophilicity of the initiator used (KPS vs AIBN), resulting in Pickering stabilized particles when AIBN was used. Upon drying the hybrid latexes showed a pH-buffering ability. Also for pH-buffering applications Jeng et al. [24] synthesized oil-in-water Pickering stabilized polyanyline dispersions using THF or Toluene as oil-phase.

Modified ZnO nanoparticles have been also incorporated into polymeric dispersions using miniemulsion polymerization. Zhang et al. [22] used ZnO nanoparticles modified with methoxypropyl silane (MPS) in the miniemulsion polymerization of styrene. Low solids content hybrid latexes with encapsulated and homogeneous distributions of ZnO in the polymer particles were obtained, when a high enough amount of MPS was used to modify the ZnO. When lower MPS amounts were used the nanoparticles remained at the polymer particle-aqueous phase interface like in Pickering stabilized systems. Both morphologies presented luminescence properties that were not present when bare ZnO nanoparticles were dispersed in a PS latex.

Lu et al. [19] synthesized also hybrid PS/ZnO latexes by miniemulsion polymerization using acrylic acid as comonomer and compatibilizer of the ZnO nanoparticles with the PS. Interestingly, the authors found that when the polymerization was done in the presence of cotton fabric, the UV-blocking capacity of the cotton fabric was substantially improved, with respect to blends of the fabric and the hybrid latex or the fabric and ZnO nanoparticles. The increased performance was attributed to the interaction of the carboxylic groups of the hybrid particles and the hydroxyl groups of the cotton.

In this work hydrophobically modified ZnO was incorporated into a film forming clear coat acrylic latex binder by the two-step seeded semibatch polymerization strategy developed recently by our group for CeO_2. Latexes with 40 wt% solids content were produced and the UV-blocking capacity of the transparent hybrid films casted was assessed and compared with acrylic/CeO_2 films. Furthermore, the morphology of the hybrid particles was assessed by electron tomography (3D-TEM) and unlike in previous works, it was unambiguously proved that most of the ZnO aggregates were encapsulated in the polymer particles.

2. Experimental

2.1. Materials

The hydrophobic ZnO nanoparticles dispersion (in methoxypropyl acetate) was kindly supplied by Altana (Germany) with 40 wt% of nanoparticles. The dispersion was dried (at 60 °C for 2 days) and the resulting powder grinded. Methyl methacrylate, MMA (Quimidroga) and n-Butyl acrylate, BA (Quimidroga) were used as received. Potassium persulfate (KPS, Aldrich) initiator was used as supplied. Dodecyl diphenyloxide disulfonate (Dowfax 2A1 45%, Dow Chemical) and n-Octadecyl acrylate (OA, 97%, Aldrich) were used as an anionic emulsifier and as a co-stabilizer, respectively. Deionized

water (MiliQ quality) was used in the miniemulsions and hydroquinone (Aldrich) was used for stopping the reaction in the samples withdrawn from the reactor.

2.2. Characterization methods

ZnO nanoparticle, polymer particle and monomer droplet size distributions were measured by Dynamic Light Scattering (DLS) using a Zetasizer Nano Series (Malvern Instrument). For this analysis, a fraction of latex (or miniemulsion) was diluted with deionized water, whereas in the case of the ZnO nanoparticles dispersions they were measured as received. The reported average particle size (droplet size) values represent an average of two repeated measurements. The stability of the miniemulsions was studied by measuring the light backscattered at 60° in the Turbiscan Lab expert equipment. Conversion was measured by gravimetric analysis.

The morphology and particle size distribution (PSD) of the latex particles as well as the morphology of the films casted from the latexes were analyzed by Transmission Electron Microscopy (TEM), TECNAI G2 20 TWIN (FEI), operating at an accelerating voltage of 200 keV in a bright-field image mode. The samples were diluted and dried using a UV lamp. The films casted at room temperature were trimmed using an ultramicrotome device at −40 °C (Leica EMFC6) equipped with a diamond knife. The ultrathin sections (100 nm) were placed on 300 mesh copper grids and were observed without further staining. 500 polymer and ZnO particles were counted and measured using a commercially available software (Image Pro Plus 7.0).

The preparation of the miniemulsion samples for cryo-TEM, involved first a vitrification procedure on a FEI Vitrobot Mark IV (Eindhoven, The Netherlands). One drop of the sample solution (~3 μL) was deposited in a copper grid (300 mesh Quantifolis, hydrophilized by glow-discharged treatment just prior to use) within the environmental chamber of the Vitrobot and the excess liquid was blotted away. The sample was shot into melting (liquid) ethane and transferred to a Single Tilt Cryo-Holder. The Cryo-Holder was previously prepared by 655 Turbo Pumping Station to maintain the sample bellow – 170 °C and to minimize the thermal derive. The sample was examined in the TECNAI G2 20 TWIN (FEI) mentioned above, operating at an accelerating voltage of 200 keV in a bright-field and low-dose image mode.

In order to assess the degree of encapsulation of the ZnO, a 3D tomographic reconstruction of a representative area of the sample was carried out using micrographs acquired in a JEOL JEM-1230 thermionic emission TEM microscope at 100 keV with a digital camera in low dose conditions. The tilt series was acquired from −60° to +60° every 2°, at nominal magnification of ×20 K and ×30 K. The images were then aligned using the IMOD 4.3.4 software package [27]; and the aligned tilt series were reconstructed using the WBP reconstruction algorithm with the TOMO3D software [28]. After the reconstruction, a post-processing of the images was carried out in Fiji [27].

2.3. Miniemulsion preparation and seeded semibatch polymerization

In a typical formulation 8.7 g of ZnO dispersion (5 weight based on monomers percent, wbm%, of ZnO) was added to MMA (30 g), BA (30 g) and OA (2.47 g) to produce the oil phase; it was stirred for 15 min under magnetic agitation. On the other hand, the water phase was produced by mixing 1.33 g of Dowfax 2A1 with 140 g of water. Then both

phases were mixed for 15 min and sonified for 15 min (operating at 8-output control and 80% duty cycle in an ice bath and under magnetic stirring) to produce the miniemulsion.

The previously prepared 30 wt% solids content (SC) miniemulsions were polymerized batchwise in a 1 L glass jacketed reactor fitted with a reflux condenser, sampling device, N_2 inlet and a stirrer rotating at 150 rpm. The miniemulsion was charged in the reactor and after reaching the desired temperature (75 °C) a shot of KPS initiator (0.3 g) was added. The reaction was carried out for half an hour. Once the seed was produced, another shot of KPS (1 g) was added to the reactor and the feeding of a preemulsion (81.4 g MMA, 81.4 g BA, 3.6 g Dowfax 2A1 and 187.2 g of water) containing the rest of the monomer needed to reach 40 wt% SC was started. The preemulsion was fed for 4 h and the reaction mixture was cooked for one more hour at 90 °C.

3. Results and discussion

3.1. ZnO nanoparticles wettability

As it has been explained in the introduction, the wettability of the nanoparticles in the monomer mixture is a key aspect affecting considerably the final morphology of the hybrid material. For that, 1 wbm% of ZnO nanoparticles were dispersed in the monomer mixture composed of MMA/BA (50/50 wt%). Fig. 1 presents the hybrid dispersion obtained.

Fig. 1. Dispersion of the ZnO nanoparticles in MMA/BA 50/50 wt% monomer mixture.

ZnO nanoparticles did not sediment in the bottom of the flask, but as it can be seen the dispersion was opaque. The reason can be found in the ZnO particle size. According to the DLS, the average diameter of the ZnO nanoparticles was 75 nm. Fig. 2 presents the TEM micrographs of this dispersion. The micrographs show that individual ZnO nanoparticles (25–35 nm) aggregated to form larger size entities in agreement with the average value measured by DLS.
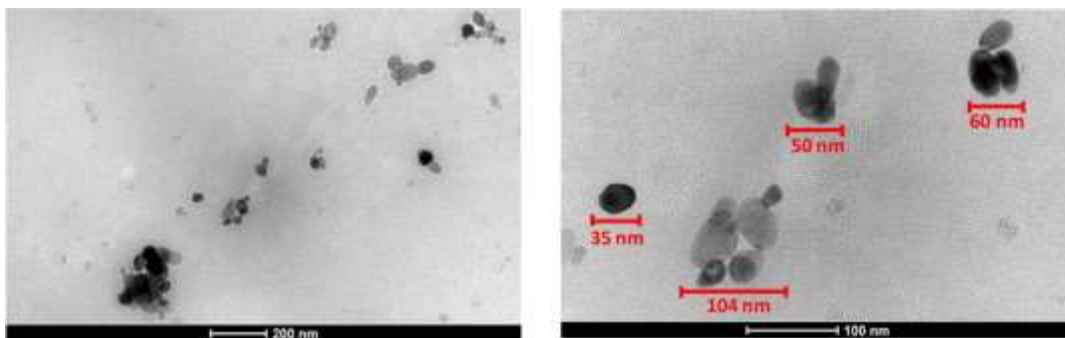
Fig. 2. TEM micrographs of 1 wt% ZnO nanoparticles in MMA/BA (50/50 wt%).

3.2. Polymerization of the hybrid latexes

The previously described two-step seeded semibatch emulsion copolymerization strategy was applied to produce hybrid acrylic/ZnO latexes. In order to produce hybrid latexes with the highest ZnO nanoparticle incorporation efficiency and the lowest coagulum content, several process variables were varied such as the way ZnO nanoparticles were incorporated (directly as received; dispersed in methoxypropyl acetate or as powder after drying out for 2 days at 60 °C) or the emulsifier amount used in the seed polymerization (1 or 2 wbm%). The obtained coagulum values were in good agreement with the miniemulsion stability measurements (see Supporting Information), showing that the reaction carried out with 1 wbm% of Dowfax in the seed and adding the ZnO directly as received (in the dispersion with methoxypropyl acetate) presented good miniemulsion stability and no coagulum in the final latex.

The final average polymer particle size of the hybrid latex (measured by DLS) was 392 nm, almost 100 nm higher than the one that should have been obtained from an homogeneous distribution of the fed monomer among the seed particles (dp$_{seed}$: 152 nm). This is an indication of particle aggregation/coagulation during the feeding step that is analyzed below with the help of TEM measurements. Another interesting result was that the gel content was 31% in the final latex. Previous works have shown that for a typical seeded semibatch emulsion polymerization formulation of MMA/BA 50/50 wt%, after the cooking period the gel content hardly exceeds 10–15% [29], [30]. The higher gel content obtained in this process may be associated to the above mentioned partial coagulation of particles (i.e., larger sizes of the polymer particles), which would increase the average number of radicals per particle, the probability of bimolecular termination and hence of gel formation [31].

3.3. Morphology of the acrylic/ZnO hybrid latexes

Fig. 3 presents the TEM micrographs for the polymerization discussed above. The micrographs present the hybrid MMA/BA/ZnO hybrid nanodroplet dispersion (a), the seed hybrid latex (b) and the final hybrid latex after the semibatch addition of the preemulsion (c).
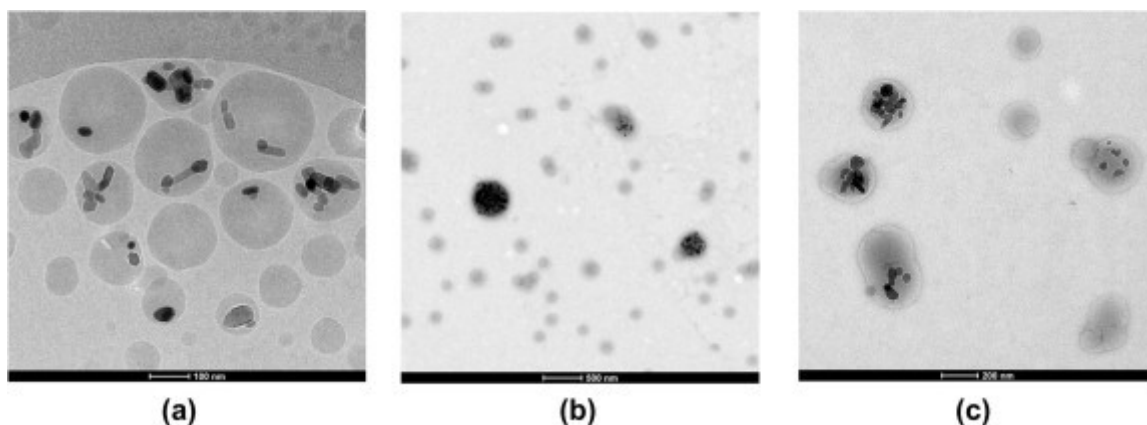
(a)   (b)   (c)

Fig. 3. (a) Cryo-TEM micrograph of the acrylic/ZnO hybrid miniemulsion, (b) TEM micrograph of the hybrid acrylic/ZnO seed and (c) TEM micrograph of the hybrid acrylic/ZnO final latex.

As it can be seen, the monomer droplet size distribution was very broad (Figs. 3 and 4a). Overall, 50% (see Fig. 3a) of the droplets contained ZnO nanoparticles or aggregates. ZnO nanoparticles appeared aggregated as had already been seen in the monomer mixture (see Fig. 2). Therefore the sonication process led to a very heterogeneous distribution of the ZnO aggregates; both large and small droplets can be identified with and without ZnO. Bourgeat-Lami et al. [32] observed a similar type of distribution for silica nanoparticles in MMA and BA monomers. They stated that a droplet with nanoparticles can be fragmentated giving smaller droplet sizes, which some of them might contain the nanoparticles and others not. Note that the production of a nanodroplet dispersion with each droplet containing one nanoparticle or aggregate of the inorganic material is not an easy task. Matching the number of droplets and the number of inorganic nanoparticles requires an accurate control of the size of the nanodroplets, which is controlled by a large number of process variables (e.g., the energy applied to the coarse emulsion, the viscosity of the organic phase, the stability of the formed nanodroplets with respect to Ostwald ripening and coalescence that depends on the composition of the organic phase (e.g., costabilizer and hydrophobe used) and the surfactant amount and type) that makes this task challenging in many circumstances. In comparison with the morphology of hybrid miniemulsions prepared with CeO_2 [33], [34], these obtained with ZnO showed a less homogeneous distribution of the ZnO and a higher aggregation of the nanoparticles.
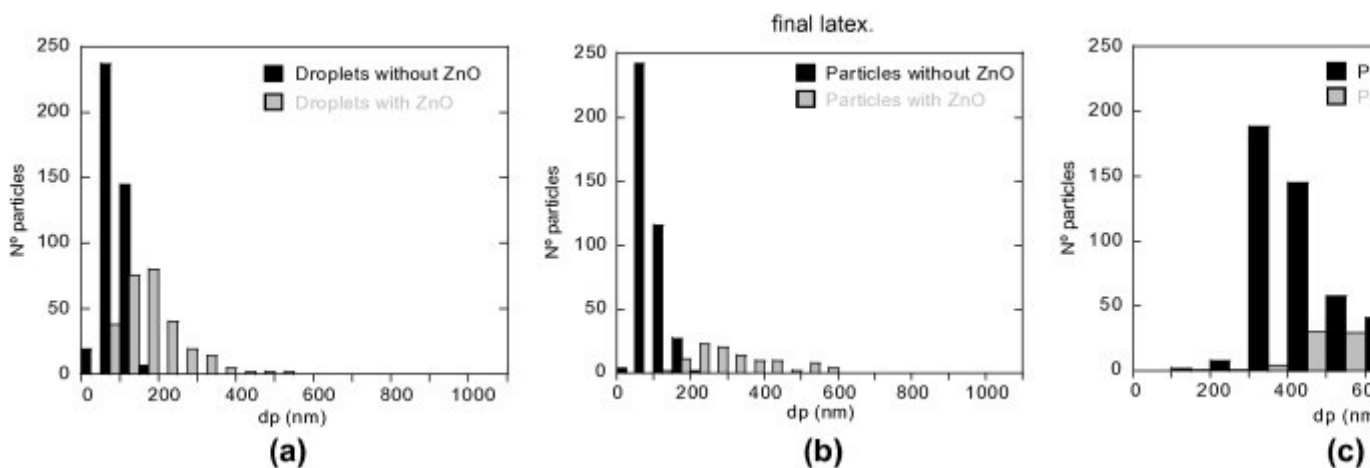

(a)   (b)   (c)

Fig. 4. PSD measured using TEM micrographs for the (a) miniemulsion droplets, (b) seed particles and (c) final particles.

Fig. 3b presents the morphology of the hybrid seed particles obtained after polymerizing the miniemulsion for 30 min. Two main populations can be distinguished, a population of large polymer particles containing ZnO and a population with smaller particles without ZnO. The comparison of the miniemulsion droplet size distribution (Fig. 4a) and the PSD of the seed latex (Fig. 4b) indicates that a substantial fraction of small droplets did not nucleate, but degraded (diffusing the monomer to the existing particles) increasing the size of the existing polymer particles. The number of particles containing ZnO was smaller (33%) than the number of monomer droplets that contained ZnO, which is an indication that in addition to the transfer of monomer from small droplets to larger ones (due to Ostwald ripening), there was also coagulation between droplets containing ZnO aggregates. Figs. 3c and 4c present the TEM micrograph and PSD of the final latex. The figures clearly indicate that growth occurred by polymerization of the entering monomer in the seed particles and coagulation/aggregation of the particles. The average particle size was well above that expected in absence of coagulation and the TEM analysis (Fig. 4c) shows the presence of very large particles (600–1000 nm) containing ZnO. The percentage of these polymer particles (21%) was slightly smaller than those found in the seed particles proving that the coagulation among polymer particles containing ZnO occurred.

The morphology of the polymer particles containing ZnO was analyzed in further detail by using electron tomography (3D-TEM). This assessment will allow to unambiguously determine the location of the ZnO nanoparticle aggregates in the final latex; namely, if the aggregates are fully encapsulated in the polymer particles or not.

Two different areas of the hybrid latex were analyzed. In the first one, a single polymer particle was analyzed which contained more than one ZnO nanoparticle (see Fig. 5a), whereas in the second region nine polymer particles with four ZnO aggregates (Fig. 5b) were studied. Each aggregate has been numbered to simplify the following discussion.
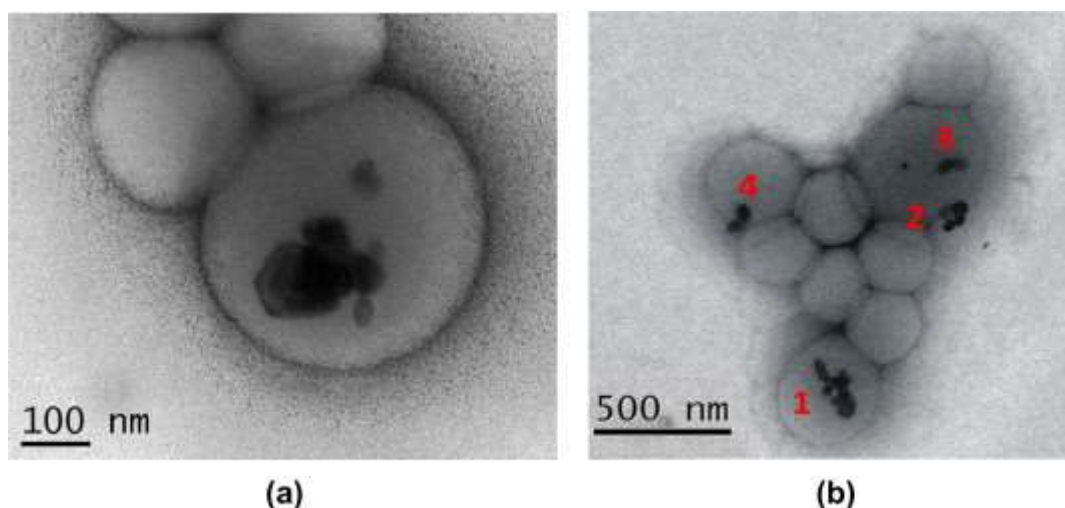

Fig. 5. TEM micrographs of two selected areas of the hybrid acrylic/ZnO latex. (a) Specimen with a single polymer particle containing ZnO. (b) Specimen with nine polymer particles and three of them containing ZnO.

Tomographic reconstructions are described in the OXYZ coordinates (Fig. 6). The OZ axis coincides with the direction of the beam and the OX axis is the tilting axis. In order to visualize this 3D object, different 2D sections are represented in the Fig. 7, Fig. 8, Fig. 9, Fig. 10. Aiming at the determination of the location of the ZnO nanoparticles inside the polymer particle, their position in different 2D sections or planes, commonly known as orthoslices was analyzed.
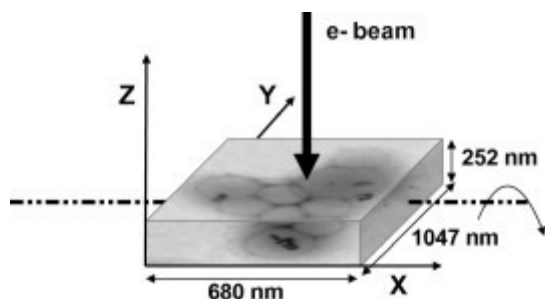

Fig. 6. Schematic representation of the *X, Y* and *Z* axis position, electron beam direction, the direction in which the sample was tilted and the dimension of the chosen sample's area.
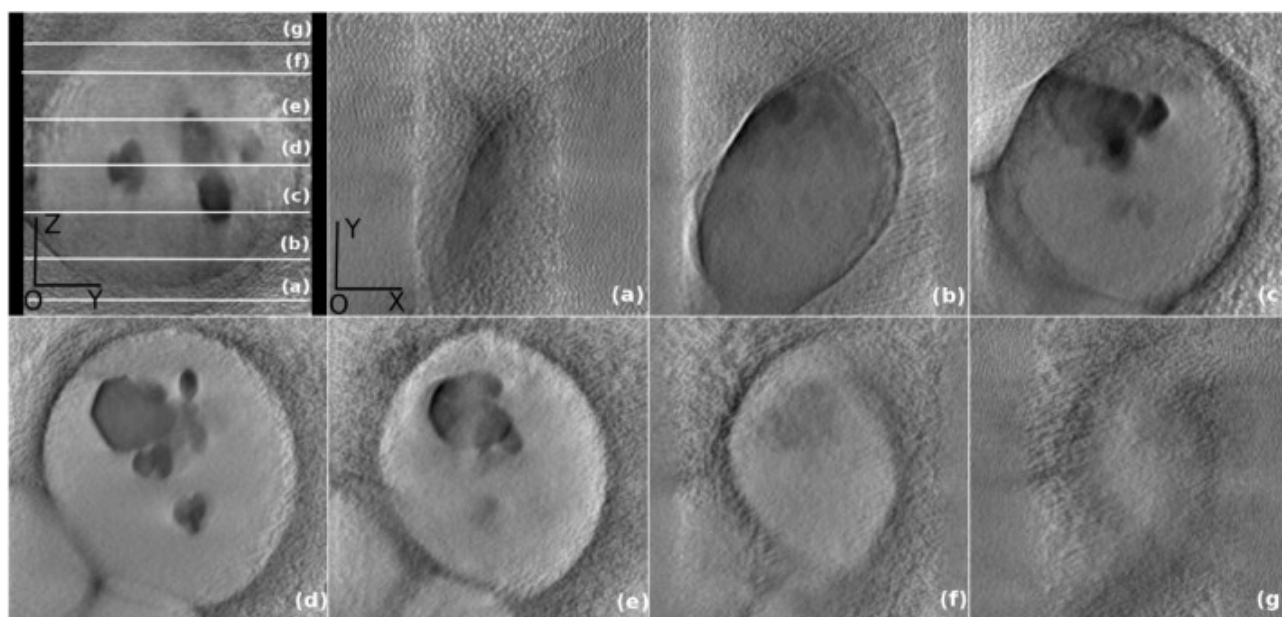
Fig. 7. Orthogonal sections of the reconstructed single particle of Fig. 5a. OXY sections corresponding to the planes indicated in the OYZ section with white lines. (a) $Z = 26$ nm; (b) $Z = 86$ nm; (c) $Z = 156$ nm; (d) $Z = 229$ nm; (e) $Z = 298$ nm; (f) $Z = 367$ nm; (g) $Z = 420$ nm.
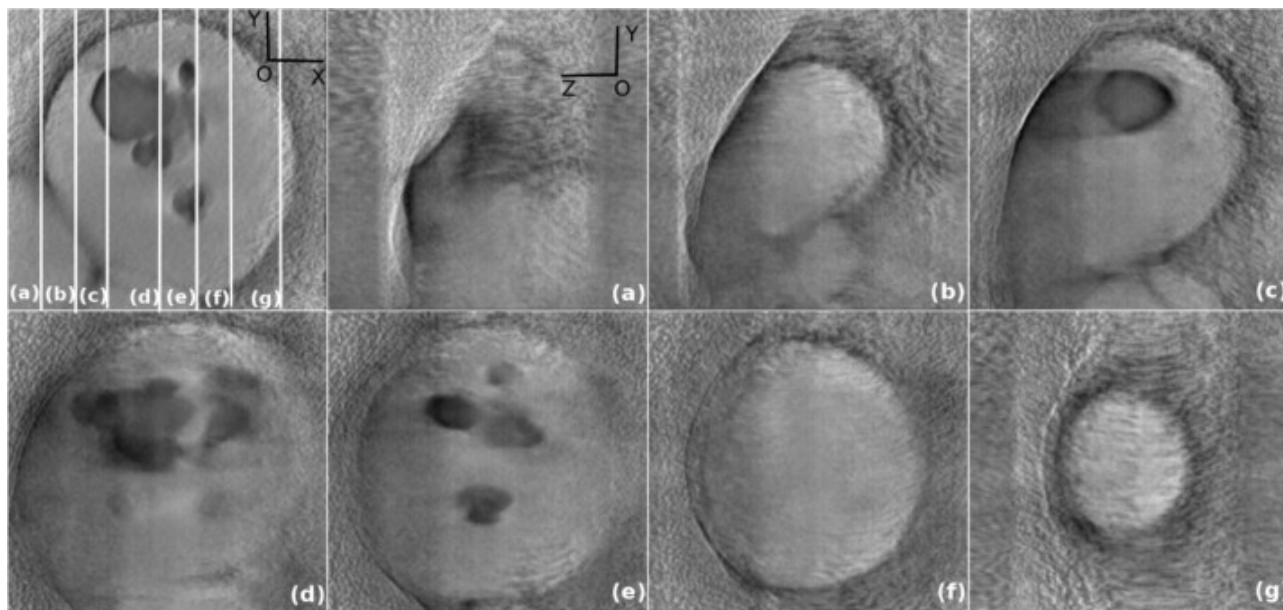
Fig. 8. Orthogonal sections of the reconstructed single particle of Fig. 5a. OYZ sections corresponding to the planes indicated in the OXY section with white lines. (a) $X = 48$ nm; (b) $X = 98$ nm; (c) $X = 141$ nm; (d) $X = 217$ nm; (e) $X = 270$ nm; (f) $X = 318$ nm; (g) $X = 318$ nm; (f) $X = 388$ nm; (g) $X = 410$ nm.
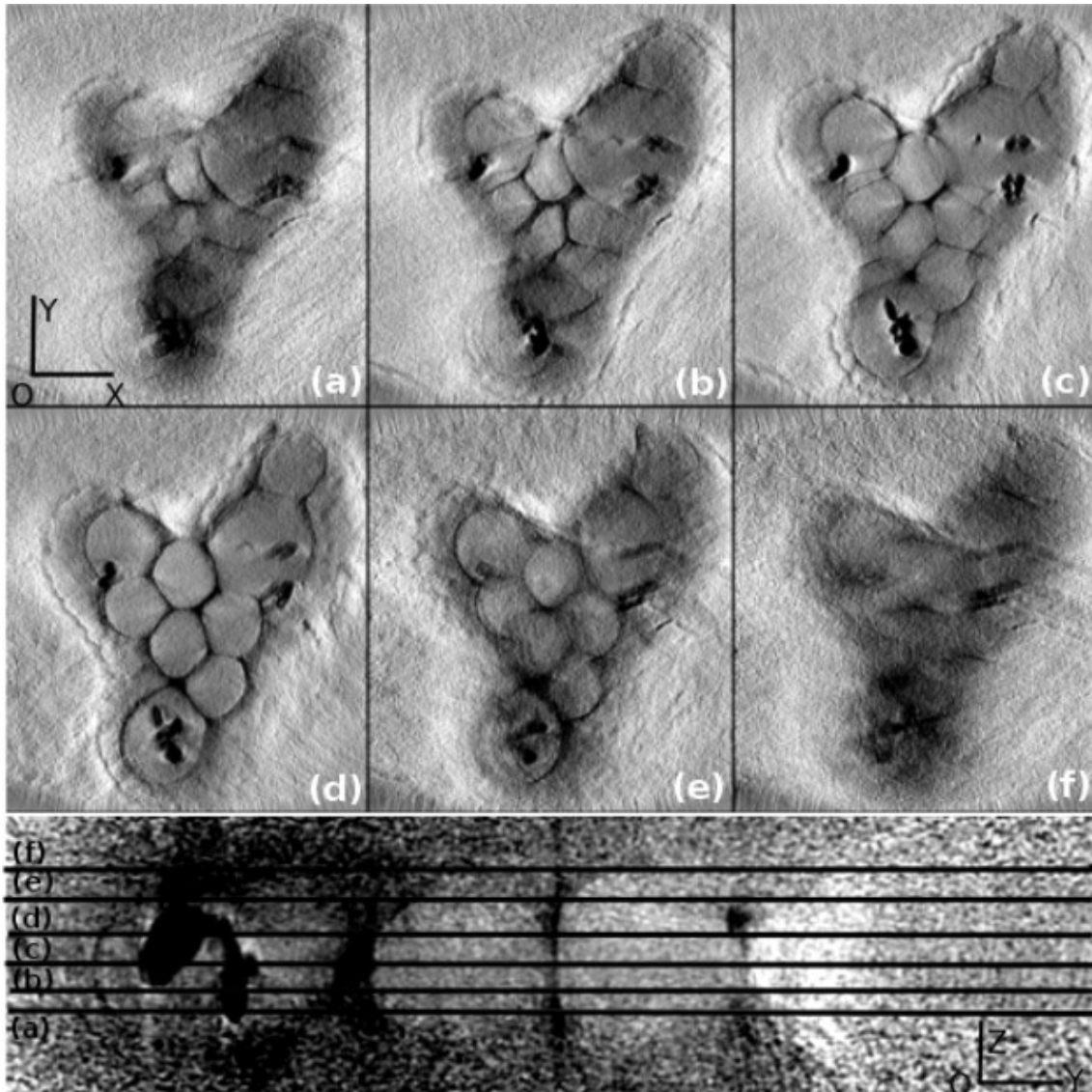
Fig. 9. Orthogonal sections of the reconstructed particles of Fig. 5b. OXY sections corresponding to the planes indicated in the OYZ section with black lines. (a) $Z = 123$ nm; (b) $Z = 156$ nm; (c) $Z = 191$ nm; (d) $Z = 235$ nm; (e) $Z = 287$ nm; (f) $Z = 330$ nm.
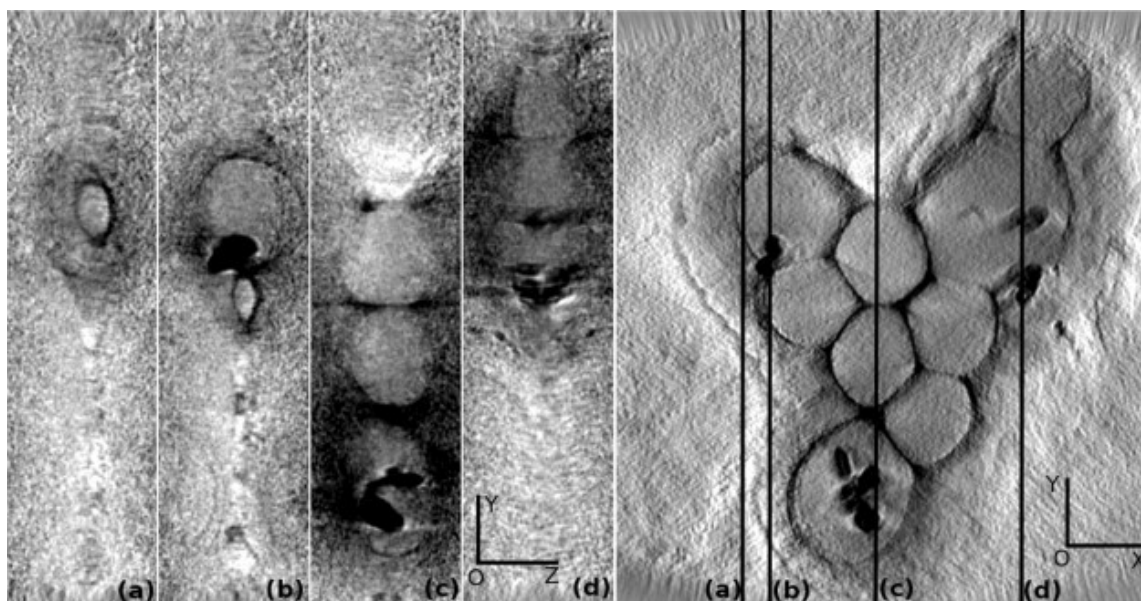
Fig. 10. Orthogonal sections of the reconstructed particles of Fig. 5b. OYZ sections corresponding to the planes indicated in the OXY section with black lines. (a) $X = 341$ nm; (b) $X = 415$ nm; (c) $X = 699$ nm; (d) $X = 1092$ nm.

In the top left image of Fig. 7 the OYZ plane of the single polymer particle (Fig. 5a) reconstruction and the corresponding OXY sections indicated with white lines are shown. From the analysis of the location of the ZnO nanoparticles through the OXY orthoslices, it is noteworthy that the aggregates were surrounded by polymer. To fulfill the interpretation and ensure the exact location of the nanoparticles, the same analysis was performed tracking the particles in the OYZ orthoslices, as shown in Fig. 8. Again, the scrutiny confirms that ZnO aggregates were encapsulated.

The reconstruction of the second specimen (Fig. 5b) was analyzed following the same procedure: the location of the ZnO nanoparticles was determined by tracking them through different orthoslices (see Fig. 9, Fig. 10). According to the orthogonal views, it can be stated that all the ZnO particles were embedded in the polymer particles. However, whereas some of them were encapsulated right in the middle of the polymer (aggregates 1 and 3 in Fig. 5b), others are located at the edges, closer to the interphase (aggregates 2 and 4 in Fig. 5b). The aggregates located on the interphase are partially embedded in the polymer particle, as can be clearly appreciated in Fig. 9 for aggregate 4. These observations come into good agreement with previous observations made from TEM micrographs. Besides, it is evident, especially in the reconstruction of the first specimen (Fig. 7, Fig. 8), that the ZnO aggregates have different dimensions and morphologies. It can be also seen in Fig. 9, Fig. 10 that the size of the polymer particles that contain ZnO aggregates were bigger than the empty ones (see also Fig. 4).

3.4. Films morphology

A potential application of these hybrid latexes is for outdoor clear coatings. A film was casted at room temperature from the hybrid latex and its cryosections were analyzed by TEM. Fig. 11 shows the TEM micrographs of the cryosectioned hybrid film at two different magnifications and the photograph of the casted film.
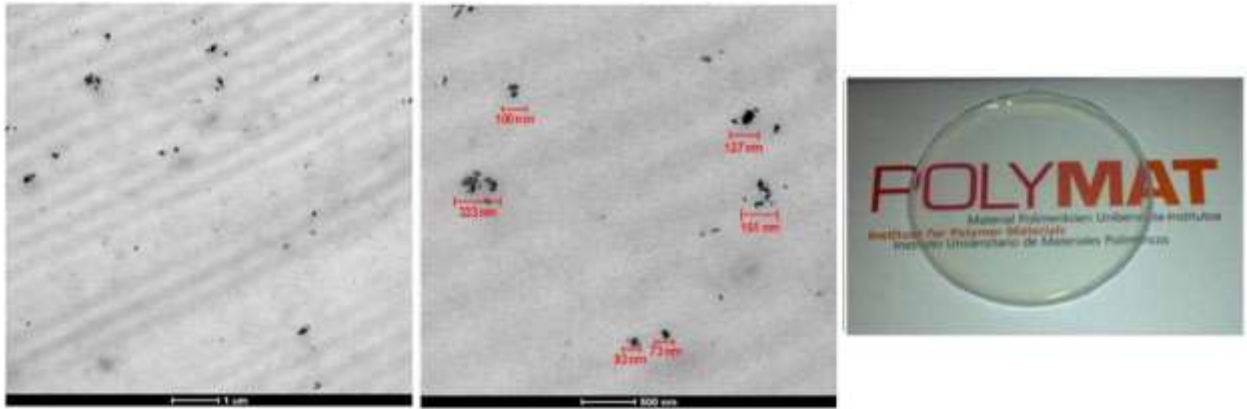
Fig. 11. TEM micrographs and photograph of the acrylic/ZnO film casted at room temperature.

Interestingly, the film was as transparent as the pristine film (without ZnO; not shown) even if the volume average ZnO aggregate size was of 95 nm (the volume distribution is presented in the Supporting Information) and the film contained 1 wt% of inorganic material. Notably, for the same amount of inorganic material ZnO produced less colored films than when CeO_2 was used [14].

For comparison purposes the UV absorbance of a pristine film and hybrid films containing the same amount (1 wt%) of ZnO or CeO_2 have been plotted in Fig. 12. Although both hybrid films presented a substantially higher UV absorption than the blank one, the absorption capacity of the acrylic/ZnO hybrid was higher and particularly higher above 350 nm, which is very appealing for UV blocking properties. It is noteworthy that in addition to the UV blocking capacity of ZnO, this semiconductor can also act as photocatalyst under UV irradiation exposure and hence can potentially degrade the polymer matrix. However, the degradation of hybrid films made with ZnO (assessed by measuring the molecular weight of the films 1 year after their preparation and exposure to sunlight) was in the range of films that did not contain ZnO; namely negligible (see the molecular weight distributions in the Supporting Information).
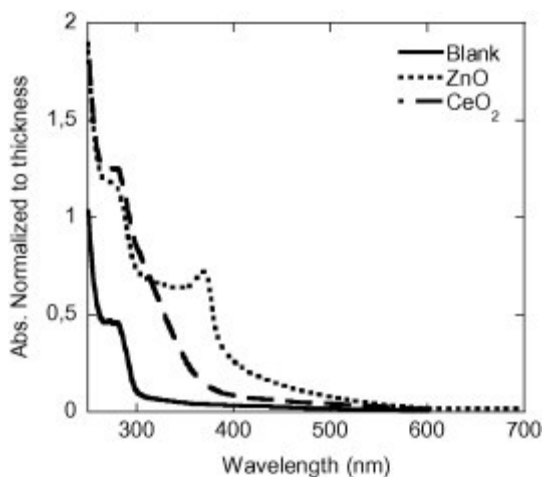

Fig. 12. UV–Vis absorption spectra of the hybrid films with the same content of inorganic material compared to that of a pristine film (without inorganic material).

4. Conclusions

Stable and coagulum free acrylic/ZnO hybrid latexes with 40 wt% solids content were obtained by a two-step seeded semibatch emulsion polymerization process, with a final ZnO loading of 1 wbm%.

In the final morphology of the acrylic/ZnO hybrid latexes, two different populations were distinguished; a population of small polymer particles without ZnO and a population with larger sizes containing aggregated ZnO nanoparticles.

When ZnO hybrid latexes were compared with analogous hybrids containing CeO_2.

Acknowledgements

References

[1] E. Bourgeat-Lami, M. Lansalot, Organic/inorganic composite latexes: the marriage of emulsion polymerization and inorganic chemistry, Adv. Polym. Sci. 233 (2010) 53–123.
[2] A.M. van Herk, Encapsulation of inorganic particles, in: J.M. Asua (Ed.), Polym. Dispersions Princ. Appl., Kluwer Academic Publisher, 1997, pp. 435–450.
[3] J.M. Asua, Miniemulsion polymerization, Prog. Polym. Sci. 27 (2002) 1283–1346. <http://linkinghub.elsevier.com/retrieve/pii/S0079670002000102>.
[4] K. Landfester, C.K. Weiss, Encapsulation by miniemulsion polymerization, Adv. Polym. Sci. 229 (2010) 1–49.
[5] J.M. Asua, Challenges for industrialization of miniemulsion polymerization, Prog. Polym. Sci. 39 (2014) 1797–1826, http://dx.doi.org/10.1016/j.progpolymsci.2014.02.009.
[6] M. Chen, L. Hu, J. Xu, M. Liao, L. Wu, X. Fang, ZnO hollow-sphere nanofilmbased high-performance and low-cost photodetector, Small 7 (2011) 2449–2453, http://dx.doi.org/10.1002/smll.201100694.
[7] F. Tiarks, K. Landfester, M. Antonietti, Silica nanoparticles as surfactants and fillers for latexes made by miniemulsion polymerization, Langmuir 17 (2001) 5775–5780, http://dx.doi.org/10.1021/la010445g.
[8] S. Cauvin, P.J. Colver, S.A.F. Bon, Pickering stabilized miniemulsion polymerization: preparation of clay armored latexes, Macromolecules 38 (2005) 7887–7889.
[9] Y. Liu, X. Chen, R. Wang, J.H. Xin, Polymer microspheres stabilized by titania nanoparticles, Mater. Lett. 60 (2006) 3731–3734, http://dx.doi.org/10.1016/j.matlet.2006.03.098.
[10] M. Micˇušik, A. Bonnefond, Y. Reyes, A. Bogner, L. Chazeau, C. Plummer, et al., Morphology of polymer/clay latex particles synthesized by miniemulsion

polymerization: modeling and experimental results, Macromol. React. Eng. 4(2010) 432–444, http://dx.doi.org/10.1002/mren.200900084.

[11] S.W. Zhang, S.X. Zhou, Y.M. Weng, L.M. Wu, Synthesis of SiO2/polystyrene nanocomposite particles via miniemulsion polymerization, Langmuir 21 (2005) 2124–2128.

[12] Y. Reyes, M. Paulis, J.R. Leiza, Modeling the equilibrium morphology of nanodroplets in the presence of nanofillers, J. Colloid Interface Sci. 352 (2010) 359–365, http://dx.doi.org/10.1016/j.jcis.2010.08.071.

[13] J.M. Asua, Mapping the morphology of polymer – inorganic nanocomposites synthesized by miniemulsion polymerization, Macromol. Chem. Phys. 215 (2014) 458–464, http://dx.doi.org/10.1002/macp.201300696.

[14] M. Aguirre, M. Paulis, J.R. Leiza, UV screening clear coats based on encapsulated CeO2 hybrid latexes, J. Mater. Chem. A 1 (2013) 3155–3162, http://dx.doi.org/10.1039/c2ta00762b.

[15] M. Aguirre, M. Paulis, J.R. Leiza, T. Guraya, M. Iturrondobeitia, A. Okariz, et al., High-solids-content hybrid acrylic/CeO2 latexes with encapsulated morphology assessed by 3D-TEM, Macromol. Chem. Phys. 214 (2013) 2157–2164.

[16] M. Aguirre, M. Paulis, J.R. Leiza, Particle nucleation and growth in seeded semibatch miniemulsion polymerization of hybrid CeO2/acrylic latexes, Polymer 55 (2014) 752–761, http://dx.doi.org/10.1016/j.polymer.2013.12.067.

[17] E.A. Meulenkamp, Synthesis and growth of ZnO nanoparticles, J. Phys. Chem. B 5647 (1998) 5566–5572.

[18] D.M. Yebra, S. Kiil, C.E. Weinell, K. Dam-Johansen, Dissolution rate measurements of sea water soluble pigments for antifouling paints: ZnO, Prog. Org. Coat. 56 (2006) 327–337, http://dx.doi.org/10.1016/j.porgcoat.2006.06.007.

[19] H. Lu, B. Fei, J.H. Xin, R. Wang, L. Li, Fabrication of UV-blocking nanohybrid coating via miniemulsion polymerization, J. Colloid Interface Sci. 300 (2006) 111–116, http://dx.doi.org/10.1016/j.jcis.2006.03.059.

[20] M.M. Demir, K. Koynov, U. Akbey, C. Bubeck, I. Park, I. Lieberwirth, et al., Optical properties of composites of PMMA and surface-modified zincite nanoparticles, Macromolecules 40 (2007) 1089–1100, http://dx.doi.org/10.1021/ma062184t.

[21] C. Petchthanasombat, T. Tiensing, P. Sunintaboon, Synthesis of zinc oxideencapsulated poly(methyl methacrylate)-chitosan core-shell hybrid particles and their electrochemical property, J. Colloid Interface Sci. 369 (2012) 52–57, http://dx.doi.org/10.1016/j.jcis.2011.12.001.

[22] J.J. Zhang, G. Gao, M. Zhang, D. Zhang, C.L. Wang, D.C. Zhao, et al., ZnO/PS core–shell hybrid microspheres prepared with miniemulsion polymerization, J. Colloid Interface Sci. 301 (2006) 78–84, http://dx.doi.org/10.1016/j.jcis.2006.05.005.

[23] J.H. Chen, C.Y. Cheng, W.Y. Chiu, C.F. Lee, N.Y. Liang, Synthesis of ZnO/polystyrene composites particles by Pickering emulsion polymerization, Eur. Polym. J. 44 (2008) 3271–3279, http://dx.doi.org/10.1016/j.eurpolymj.2008.07.023.

[24] J. Jeng, T.Y. Chen, C.F. Lee, N.Y. Liang, W.Y. Chiu, Growth mechanism and pHregulation characteristics of composite latex particles prepared from Pickering emulsion polymerization of aniline/ZnO using different hydrophilicities of oil phases, Polymer 49 (2008) 3265–3271, http://dx.doi.org/10.1016/j.polymer.2008.05.027.

[25] S.K. Dhoke, A.S. Khanna, T.J.M. Sinha, Effect of nano-ZnO particles on the corrosion behavior of alkyd-based waterborne coatings, Prog. Org. Coat. 64 (2009) 371–382, http://dx.doi.org/10.1016/j.porgcoat.2008.07.023.

[26] M. Xiong, G. Gu, B. You, L. Wu, Preparation and characterization of poly(styrene butylacrylate) latex nano-ZnO nanocomposites, J. Appl. Polym.

Sci. 90 (2003) 1923–1931.

[27] J.R. Kremer, D.N. Mastronarde, J.R. McIntosh, Computer visualization of threedimensional image data using IMOD, J. Struct. Biol. 116 (1996) 71–76, http://dx.doi.org/10.1006/jsbi.1996.0013.

[28] J.I. Agulleiro, J.J. Fernandez, Fast tomographic reconstruction on multicore computers, Bioinformatics 27 (2011) 582–583, http://dx.doi.org/10.1093/bioinformatics/btq692.

[29] I. Gonzalez, J.M. Asua, J.R. Leiza, The role of methyl methacrylate on branching and gel formation in the emulsion copolymerization of BA/MMA, Polymer 48 (2007) 2542–2547, http://dx.doi.org/10.1016/j.polymer.2007.03.015.

[30] O. Elizalde, G. Arzamendi, J.R. Leiza, J.M. Asua, Seeded semibatch emulsion copolymerization of n-butyl acrylate and methyl methacrylate, Ind. Eng. Chem. Res. 43 (2004) 7401–7409.

[31] M.J. Barandiaran, J.C. De la Cal, J.M. Asua, Emulsion polymerization, in: J.M. Asua (Ed.), Polym. React. Eng., Blackwell Publishing, 2007, pp. 233–269.

[32] E. Bourgeat-Lami, G.A. Farzi, L. David, J.-L. Putaux, T.F.L. McKenna, Silica encapsulation by miniemulsion polymerization: distribution and localization of the silica particles in droplets and latex particles, Langmuir 28 (2012) 6021–6031, http://dx.doi.org/10.1021/la300587b.

[33] M. Paulis, J.R. Leiza, Encapsulation with miniemulsion polymerization, in: S. Kabayashi, K. Mullen (Eds.), Encycl. Polym. Nanomater., Springer-Verlag, 2014. 10.1007/987-3-642-36199-9_261-1.

[34] M. Aguirre, M. Paulis, M. Barrado, M. Iturrondobeitia, A. Okariz, T. Guraya, et al., Evolution of particle morphology during hybrid acrylic/CeO2 nanocomposites produced by miniemulsion polymerization, J. Polym. Sci. Part A: Polym. Chem.53 (2015) 792–799, http://dx.doi.org/10.1002/pola.27504.